ACS OMEGA

http://pubs.acs.org/journal/acsodf

Article

Charge Transfer and Level Lifetime in Molecular Photon-Absorption upon the Quantum Impedance Lorentz Oscillator

Qi-Qi Bai, Zheng-Ji Fang, Xiao-Feng Wang, Yong Zhang,* Xing-Hua Zhao,* and Pei-De Zhao*

Cite This: *ACS Omega* 2023, 8, 19950−19962

Read Online

ACCESS | Metrics & More | Article Recommendations

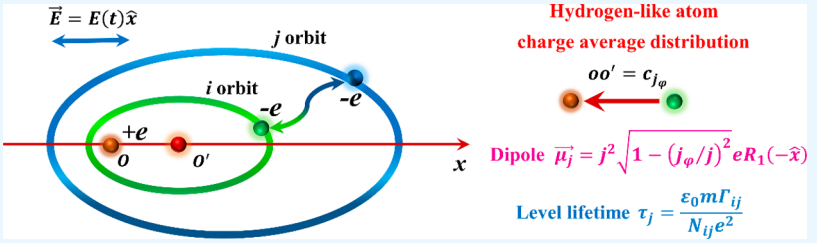

ABSTRACT: On the strength of the new quantum impedance Lorentz oscillator (QILO) model, a charge-transfer method in molecular photon-absorption is proposed and imaged via the numerical simulations of 1- and 2-photon-absorption (1PA and 2PA) behaviors of the organic compounds LB3 and M4 in this paper. According to the frequencies at the peaks and the full width at half-maximums (FWHMs) of the linear absorptive spectra of the two compounds, we first calculate the effective quantum numbers before and after the electronic transitions. Thus, we obtain the molecular average dipole moments, i.e., 1.8728×10^{-29} C·m (5.6145 D) for LB3 and 1.9626×10^{-29} C·m (5.8838 D) for M4 in the ground state in the tetrahydrofuran (THF) solvent. Then, the molecular 2PA cross sections corresponding to wavelength are theoretically inferred and figured out by QILO. As a result, the theoretical cross sections turn out to be in good agreement with the experimental ones. Our results reveal such a charge-transfer image in 1PA near wavelength 425 nm, where an atomic electron of LB3 jumps from the ground-state ellipse orbit with the semimajor axis $a_i = 1.2492 \times 10^{-10}$ m = 1.2492 Å and semiminor axis b_i = 0.4363 Å to the excited-state circle ($a_j = b_j$ = 2.5399 Å). In addition, during its 2PA process, the same transitional electron in the ground state is excited to the elliptic orbit with a_j = 2.5399 Å and b_j =1.3808 Å, in which the molecular dipole moment reaches as high as 3.4109×10^{-29} C·m (10.2256 D). In addition, we obtain a level-lifetime formula with the microparticle collision idea of thermal motion, which indicates that the level lifetime is proportional (not inverse) to the damping coefficient or FWHM of an absorptive spectrum. The lifetimes of the two compounds at some excited states are calculated and presented. This formula may be used as an experimental method to verify 1PA and 2PA transition selection rules. The QILO model exhibits the advantage of simplifying the calculation complexity and reducing the high cost associated with the first principle in dealing with quantum properties of optoelectronic materials.

1. INTRODUCTION

Molecular charge-transfer (CT) refers to a charge redistribution process in space when an excited molecule or atom transits from its initial stable or metastable state to the final state. During this process, the electric dipole moment of the microscopic particle will change to some extent, leading to varying the electrical or optical properties of the molecular material. CT is a common phenomenon in physical and chemical reactions.[1−4] Due to its rich dynamic behavior in the study of chemistry and physics,[5−10] charge-transfer plays an important role in many basic research and technical applications such as nanomanufacturing,[11,12] catalytic reaction,[13,14] and plasma-surface interaction.[15] Back in the 1950s, Hagstrum opened up the CT research field by developing ion neutralization spectroscopy and made a key discussion of CT mechanisms and related kinetic processes.[16] Since then, building on earlier research achievements, considerable progress has been made in CT studies. Some important views on CT are briefly stated as follows.

The classical Marcus theory was originally used to study the mechanism of electron transfer reactions in the outer layers. Although the Marcus theory has had some success in predicting charge transport in organic materials, it is not yet suitable for low-temperature high-frequency or low-frequency high-temperature conditions because it does not consider quantum effects of the molecule or atom.[17] In the early 1990s, Los et al. reviewed the general nature of CT

Received: March 21, 2023
Accepted: May 5, 2023
Published: May 22, 2023

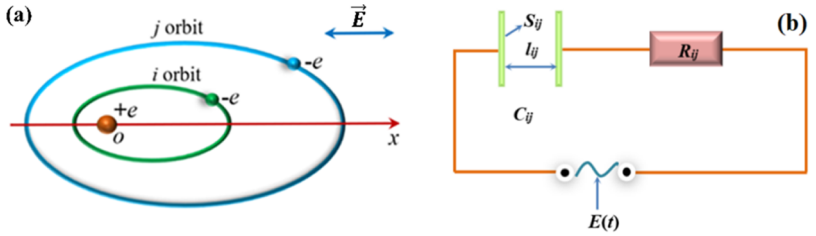

Figure 1. Quantum impedance acting on the driven outermost jumping electron between two energy levels of E_i and E_j. (a) Level i to j transition orbits of the outermost jumping electron of a hydrogen-like atom. (b) Circuit diagram of quantum impedance $Z_{ij} = R_{ij} + 1/(i'\omega C_{ij})$ on the jumping electron.

research.[18] Gauyacq and Borisov presented the CT process in atom−metal surface collisions, focusing on the modifications of this process induced by the presence of adsorbates on the surface.[19] Valeri and Monreal pointed out that Auger charge-transfer is an inelastic two-electron tunneling process accompanied by Auger electron emission.[20,21] The photo-induced charge-transfer[22−25] is also one type of CT process. The charge-transfer from the donor to the acceptor will occur under light excitation, which is called intramolecular charge-transfer (ICT). The donor part and acceptor part of a molecule are usually connected by a covalent bond or a conjugate bridge. The ICT mechanism is considered to be the most basic and critical step in various photophysical and photochemical processes.[25−27] ICT is sometimes subdivided into twisted intramolecular charge transfer (TICT) and planar intramolecular charge transfer (PICT)[15,28,29] for organic molecules with different structures. In a quantitative description on the CT process, the first principle based on local density approximation (LDA) and general gradient approximation (GGA) is a common and important calculating method.[30] Nowadays, it plays a key role in the calculation of molecular charge-transfer despite facing drawbacks like a complex calculation procedure and requiring great time and cost. Currently, charge transfer along with energy transfer is a focal point due to its universality and complexity in physical and chemical reactions.

It is well known that the famous Lorentz oscillator model is widely used qualitatively in many studies[31−36] owing to its clear physical images, easy mathematical treatments, and terse explanation of the linear and nonlinear interactions of light and matter. Unfortunately, it provides only a classical insight into the light−matter interaction. The quantum impedance Lorentz oscillator (QILO) model was recently established and proposed,[37,38] in which the classical Lorentz oscillator had been quantized via the Bohr−Sommerfeld quantum theory and 1- and 2-photon-absorption selection rules of quantum mechanics. In QILO, all of its parameters including the linear parameter, the nonlinear parameter, the damping coefficient, and the oscillator strength have been expressed in terms of the typical quantum physical quantity, such as effective quantum number, Bohr radius, and the ground-state energy of the hydrogen atom. Based on the QILO model, the theoretical simulations of the 1PA spectra of atomic hydrogen and lithium and 1PA and 2PA spectra of many organic molecules turn out to be in good agreement with the experimental ones.[37]

By means of the QILO model in this paper, we try to figure out a charge-transfer image in molecular photon-absorption via numerical simulations of 1PA and 2PA behaviors of the two organic compounds of LB3 and M4. In addition, we also suggest a theoretical formula of the energy level lifetime, in which the microparticle collision idea of thermal motion will be taken into account, in accordance with the QILO model. The level lifetimes of the two compounds at some excited states have been numerically investigated in detail.

2. MOLECULAR CHARGE-TRANSFER AND LEVEL LIFETIME BASED ON THE QILO MODEL

To our knowledge, the Lorentz oscillator is used to describe the classical kinetic behavior of atomic electrons in the light−matter interaction theory very successfully. The popular model can be outlined by the following equation

$$\frac{d^2x}{dt^2} + \Gamma\frac{dx}{dt} + \omega_0^2 x - Ax^2 + Bx^3 - \cdots = -\frac{e}{m}E \tag{1}$$

where Γ is the damping coefficient, ω_0^2 is a linear parameter, A is the second-order nonlinear parameter, B is the third-order nonlinear parameter, ⋯, and E is the light electric field acting on the moving electron with e charge and m mass. As one of its applications, the outermost electronic motion of a hydrogen-like atom is treated with a Lorentz oscillator. As we know, a hydrogen-like atom may play a key role in molecular formation because one kind of molecular chemical bond is duplet shared by two adjacent hydrogen-like atoms in a molecule. The Lorentz oscillator, however, is not available for the quantitative description of light−matter interaction due to its lack of quantum idea or more specifically because it does not consider an energy level structure of any atom.

As a newly quantized Lorentz oscillator, the key idea of QILO is that a spherical capacitor with quantum capacity C_{ij} is substituted for a hydrogen-like atom with the energy level structure in view of their very same behavior of energy storage during the outermost electronic transition process from level i to j. Here, C_{ij} is determined by the following relation

$$\hbar\omega_{ij} = E_j - E_i = \frac{e^2}{2}\frac{1}{4\pi\varepsilon_0 a_i} - \frac{e^2}{2}\frac{1}{4\pi\varepsilon_0 a_j} = \frac{e^2}{2C_{ij}} \tag{2}$$

where

$$C_{ij} = 4\pi\varepsilon_0\frac{a_i a_j}{a_j - a_i} \tag{3}$$

exactly represents the electric capacity of a spherical capacitor with inside radius a_i and outside radius a_j. According to the Bohr−Sommerfeld model of a hydrogen-like atom, in an adiabatic approximation, the semimajor axis, the semiminor axis, and the total energy of the atomic outermost electron in eqs 2 and 3 are, respectively,

https://doi.org/10.1021/acsomega.3c01922
ACS Omega 2023, 8, 19950−19962

$$a_n = n^2 R_1 \tag{4}$$

$$b_n = n n_\varphi R_1 = b_{n_\varphi} \tag{5}$$

and

$$E_n = \frac{E_1}{n^2} = -\frac{e^2}{2}\frac{1}{4\pi\varepsilon_0 a_n} \tag{6}$$

where R_1 is the Bohr radius, E_1 is the ground-state energy of the hydrogen atom, and n and n_φ are, respectively, the effective principal quantum number and the effective angle quantum number, i.e., n and n_φ can be a positive noninteger quantum number in consideration of the quantum deficit representing the situation of the penetrating orbits in a hydrogen-like atom. Accordingly, the impedance on the outermost jumping electron of a hydrogen-like atom during its transition process from level i to j shown in Figure 1a is $Z_{ij} = R_{ij} + 1/(i'\omega C_{ij})$. Its circuit diagram is shown in Figure 1b, where R_{ij} is the quantum resistance and $1/(i'\omega C_{ij})(i' = \sqrt{-1})$ is the quantum capacitance for the circular frequency ω of the interactive light field $\overline{E}(t) = E_x(t)\overline{i} = E(t)\overline{i}$ along the x (long-axis) direction.

Relative to the kernel at the origin O as the left focus of the ellipse orbit of Figure 1a, the electronic movement along the long axis (x direction) of Bohr−Sommerfeld orbits can be treated as an anharmonic Lorentz oscillator. In addition, for a circle orbit, its movement along the diameter can be regarded as a harmonic one. Particularly, the electronic transition process from level i to j can be considered a resonance one of the damped forced vibration of the Lorentz oscillator with the quantum impedance Z_{ij} under an external light field. As a result of the energy transformation and conservation law, the kinematic equation of QILO can be expressed as

$$\frac{d^2x}{dt^2} + \Gamma_{ij}\left(1 - i'\frac{1}{R_{ij}C_{ij}\omega}\right)\frac{dx}{dt} + \omega_j^2 x - A_j x^2 + B_j x^3 - \cdots = -\frac{e}{m}E \tag{7}$$

Thus, the transition process of a hydrogen-like atom can be simply treated with a syntony behavior of QILO under the electric field of light.

Based on the QILO model, all parameter expressions in eq 7 are summarized as follows. The damping coefficient

$$\Gamma_{ij}(i_\varphi, j_\varphi) = \sqrt{2}\pi\left\{\left[R_1 j^2\sqrt[3]{\left(\frac{j_\varphi}{j}\right)^2} + \delta R'\right]^2 - \left[R_1 i^2\sqrt[3]{\left(\frac{i_\varphi}{i}\right)^2} + \delta R'\right]^2\right\}\overline{v}N' \tag{8}$$

where $\overline{v}$ is the mean velocity of the electronic thermal motion at a given temperature, N' is the environment atom (or molecule) number density, R' is the effective radius of the globe representing the environment atom or molecule colliding with the jumping electron, and δ is an adjustable constant depending on the state of matter. Usually, $\delta = 1$ for the gaseous state, and $\delta \sim 0.9$ for the liquid state in view of the size exclusion between molecules. It should be noted that in eq 7 the damping coefficient $\Gamma_{ij} = 0$ when $i = j$. By way of Taylor series expansion of the long-axis component of the kernel's Coulomb force acting on the moving electron as the QILO restoring force, the linear parameter

$$\omega_j^2 = k_j'(j_\varphi)/m = \omega_j^2(j_\varphi) = \frac{\omega_1^2(j_\varphi = j)}{j^6}\left\{1 + 3\left[1 - \left(\frac{j_\varphi}{j}\right)^2\right] + 6\left[1 - \left(\frac{j_\varphi}{j}\right)^2\right]^2\right\} \tag{9}$$

$$\omega_1^2(j_\varphi = j) = \frac{e^2}{4\pi\varepsilon_0 m R_1^3} = 1.7 \times 10^{33}\ (\mathrm{SI}) \tag{10}$$

the second-order nonlinear parameter

$$A_j = A_j(j_\varphi) = A_j'(j_\varphi)/m = \frac{A_1}{j^8}\left\{3\left[1 - \left(\frac{j_\varphi}{j}\right)^2\right]^{1/2} + 12\left[1 - \left(\frac{j_\varphi}{j}\right)^2\right]^{3/2}\right\} \tag{11}$$

$$A_1 = \frac{e^2}{4\pi\varepsilon_0 m R_1^4} = 3.2 \times 10^{43}\ (\mathrm{SI}) \tag{12}$$

the third-order nonlinear parameter

$$B_j = B_j(j_\varphi) = B_j'(j_\varphi)/m = \frac{B_1}{j^{10}} \times 6 \times \left[1 - \left(\frac{j_\varphi}{j}\right)^2\right] \tag{13}$$

$$B_1 = \frac{e^2}{4\pi\varepsilon_0 m R_1^5} = 6.1 \times 10^{53}\ (\mathrm{SI}) \tag{14}$$

where $j_\varphi = j, j - 1, j - 2, \cdots$.[37]

A possible orbit of the outermost electron of a hydrogen-like atom at an excited state with the effective quantum numbers j and j_φ is schematically shown in Figure 2, in which

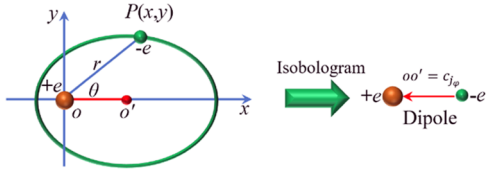

Figure 2. Electronic elliptic orbit of a hydrogen-like atom in the bound state and its equivalent charge distribution in space.

the coordinate origin O situates at the left focus of the ellipse orbit, and O' represents the ellipse center. The orbit equation of the electronic movement is

$$\frac{(x - c_{j_\varphi})^2}{a_j^2} + \frac{y^2}{b_{j_\varphi}^2} = 1 \tag{15}$$

where $c_{j_\varphi} = oo' = \sqrt{a_j^2 - b_{j_\varphi}^2}$ represents the focal length of the ellipse. The average charge distribution in space for a hydrogen-like atom at the j level is just like an electric dipole

https://doi.org/10.1021/acsomega.3c01922
ACS Omega 2023, 8, 19950−19962

shown in Figure 2. Thus, the atomic electric dipole moment can be estimated by using the following expression

$$\mu_j = ec_{j_\varphi} = e\sqrt{a_j^2 - b_{j_\varphi}^2} = \mu_{j_\varphi} \tag{16}$$

Using eqs 4 and 5 in eq 16, we can get

$$\mu_{j_\varphi} = j^2\sqrt{1 - (j_\varphi/j)^2}\, eR_1 \tag{17}$$

$$\begin{aligned} eR_1 &= 1.602 \times 10^{-19} \times 0.529 \times 10^{-10} \\ &= 8.4746 \times 10^{-30}\ \text{C·m} \\ &= 2.5407\ \text{D} \\ &= 2.5407 \times 10^{-18}\ \text{esu·C·m} \end{aligned} \tag{18}$$

The vector expression of eq 16 is

$$\overrightarrow{\mu_{j_\varphi}} = j^2\sqrt{1 - (j_\varphi/j)^2}\ eR_1(-\vec{i}) \tag{19}$$

Equation 16 exhibits a new simple way of estimating the atomic or molecular electric dipole moment.

The QILO model allows us to obtain a theoretical formula of an energy level lifetime, incorporating the microparticle collision idea of thermal motion. Generally speaking, the width of the energy level of an excited atom is well known to be closely related to the level lifetime. As far as we know, the reciprocal of the level lifetime determined by the Heisenberg energy-time uncertainty is empirically assumed to be the damping coefficient in the framework of quantum mechanics. However, in fact, just as Daprà et al.[39] pointed out, only in the absence of collisions, predissociation, or autoionization can the lifetime reciprocal be considered as the damping coefficient. As thus, in dealing with most material spectra measured in room conditions, some empirical values of the damping coefficient have to be used due to the lack of its calculation formula on account of numerical simulation requirements. Luckily, for the thermal-motion collision situation, Figure 1b may indicate that there is a constant $\tau_j = R_{ij}C_{ij}$ in the QILO model, which may represent the lifetime of the transition electron at energy level j because of the usual expression $\tau = RC$ as the decay time constant in a typical RC series circuit. Thus, in light of the QILO model, we assume that the energy level lifetime of an excited hydrogen-like atom can be defined as

$$\tau_j = R_{ij}C_{ij} = \rho_{ij}\varepsilon_0 = \frac{\varepsilon_0 m\Gamma_{ij}}{e^2 N_{ij}} \tag{20}$$

where specific resistance $\rho_{ij} = m\Gamma_{ij}/(e^2N_{ij})$, in which N_{ij} is the number density of the jumping electron. It is worth noting that the level lifetime based on the QILO model is proportional (not inverse) to the damping coefficient or full width at half-maximum (FWHM) Γ_{ij} of an absorptive spectrum of the material. It means that, for a given sample, i.e., N_{ij}, the larger the damping coefficient Γ_{ij}, the longer the excited-state lifetime according to the QILO model. This result is somewhat beyond expectation. Moreover, this time interval depends on not only the excited state j but also the initial state i. As for a level lifetime of the ground state, $\tau_j = \tau_{\text{ground}} \to \infty$ owing to $N_{ij} \equiv 0$ in eq 20. On the other hand, on rewriting eq 20 as

$$N_{ij} = \frac{\varepsilon_0 m\Gamma_{ij}}{e^2\tau_j} \tag{21}$$

one may find that some sample content in the mixture may be estimated by eq 21 through the measured FWHM Γ_{ij} and the excited-state lifetime τ_j. This formula might be helpful to the elemental analysis, molecular reaction kinetics, environmental monitoring, and so on.

Taking the Fourier forms of the coordinate $x(t)$ and the interactional light $E(t)$ into eq 7, we can obtain the expression of the first-order electric susceptibility of a homogeneous medium as

$$\begin{aligned} \chi^{(1)}(\omega) &= \sum_i\sum_{j>i}\chi_{ij}^{(1)}(\omega) \\ &= \sum_i\sum_{j>i}\frac{N'_{i\to j}e^2}{\varepsilon_0 m}\frac{1}{\omega_j^2 - \Gamma_{ij}/(R_{ij}c_{ij}) - \omega^2 - i'\Gamma_{ij}\omega} \\ &= \sum_i\sum_{j>i}\frac{N'_{i\to j}e^2}{\varepsilon_0 m}F_{ij}(\omega) \end{aligned} \tag{22}$$

where

$$\begin{aligned} F_{ij}(\omega) &= \frac{1}{\omega_j^2 - \Gamma_{ij}/(R_{ij}c_{ij}) - \omega^2 - i'\Gamma_{ij}\omega} \\ &= \frac{1}{\omega_{ij}^2 - \omega^2 - i'\Gamma_{ij}\omega} \end{aligned} \tag{23}$$

$$\omega_{ij}^2 = \omega_j^2 - \Gamma_{ij}/(R_{ij}c_{ij}) = \left(\frac{E_j}{\hbar} - \frac{E_i}{\hbar}\right)^2 = \left(\frac{E_1}{\hbar}\right)^2\left(\frac{1}{j^2} - \frac{1}{i^2}\right)^2 \tag{24}$$

and

$$N'_{i\to j} = \frac{g(j)}{g(i)}N'_{i-1\to i}e^{-(E_j - E_i)/k_BT} = \frac{g(j)}{g(i)}N'_{i-1\to i}e^{-\hbar\omega_{ij}/k_BT} \tag{25}$$

named the $i \to j$ transition atom number density in the equilibrium situation between atomic emission and absorption under a light field.[37] In eq 25, $g(i)$ is the degeneracy at state i. Equation 23 shows that the damping coefficient Γ_{ij} just represents the full width at half-maximum (FWHM) of the 1PA spectrum. It can also be expressed in terms of wavelength λ as

$$\Gamma_{ij} = \frac{2\pi c\Delta\lambda_{\text{FWHM}}}{\lambda_{\text{peak}}^2}$$

where c is the light velocity in vacuum and $\Delta\lambda_{\text{FWHM}}$ is the FWHM near the spectral peak wavelength λ_{peak}. In eq 23, ω_{ij} represents the transition eigenfrequency of the hydrogen-like atom. The imaginary part and real part of the susceptibility are, respectively,

$$\begin{aligned} \chi_{\text{Im}}^{(1)}(\omega) &= \sum_i\sum_{j>i}[\chi_{ij}^{(1)}(\omega)]_{\text{Im}} \\ &= \sum_i\sum_{j>i}\frac{N'_{i\to j}e^2}{\varepsilon_0 m\omega_{ij}^2}\frac{\frac{\Gamma_{ij}\omega}{\omega_{ij}^2}}{\left[1 - \left(\frac{\omega}{\omega_{ij}}\right)^2\right]^2 + \left(\frac{\Gamma_{ij}\omega}{\omega_{ij}^2}\right)^2} \end{aligned} \tag{26}$$

https://doi.org/10.1021/acsomega.3c01922
ACS Omega 2023, 8, 19950−19962

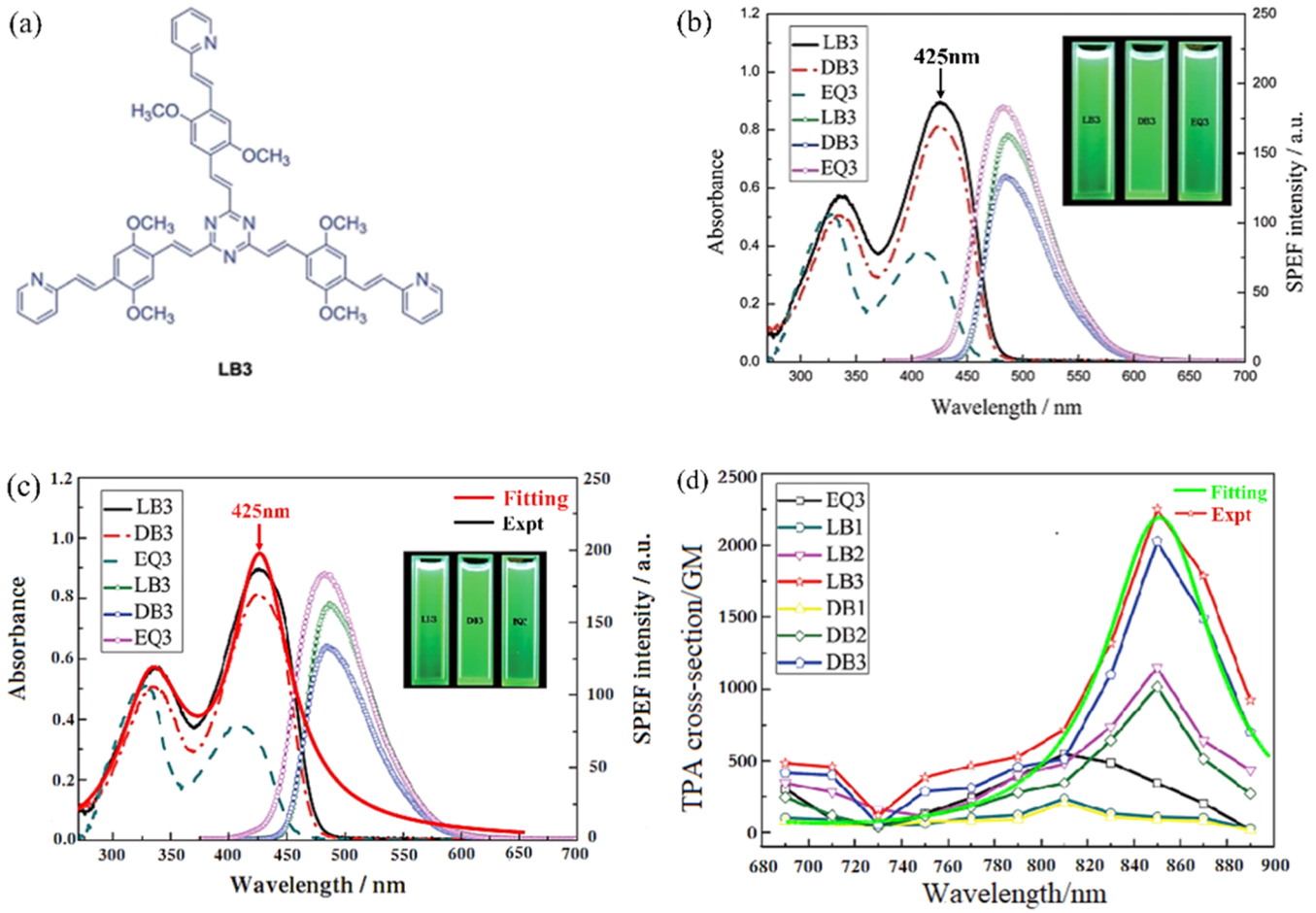

Figure 3. Experimental 1PA and 2PA (TPA) of LB3 and theoretical simulations based on the QILO model. (a) Molecular structure, (b) 1PA spectrum, (c) fitting diagram of the 1PA spectrum using QILO, and (d) experimental 2PA cross section and its numerical simulation using the QILO model (green line).

and

$$\chi_{\mathrm{Re}}^{(1)}(\omega) = \sum_i \sum_{j>i} [\chi_{ij}^{(1)}]_{\mathrm{Re}} = \sum_i \sum_{j>i} \frac{N'_{i\to j} e^2}{\varepsilon_0 m \omega_{ij}^2} \frac{1 - \left(\frac{\omega}{\omega_{ij}}\right)^2}{\left[1 - \left(\frac{\omega}{\omega_{ij}}\right)^2\right]^2 + \left(\frac{\Gamma_{ij}\omega}{\omega_{ij}^2}\right)^2} \quad (27)$$

In the situation of the stable solution of eq 7 in the time domain, we can obtain the relational expression among the atom transition eigenfrequency ω_{ij}, the angular frequency $\omega_{ij}^{\mathrm{peak}}$ at a spectrum peak, and FWHM Γ_{ij} as

$$\omega_{ij}^{\mathrm{peak}} = \omega_{ij} \sqrt{\frac{1}{3}\left(1 - \frac{\Gamma_{ij}^2}{2\omega_{ij}^2}\right) + \frac{2}{3}\sqrt{1 - \frac{\Gamma_{ij}^2}{4\omega_{ij}^2} + \frac{1}{4}\left(\frac{\Gamma_{ij}^2}{2\omega_{ij}^2}\right)^2}} \quad (28)$$

or

$$\omega_{ij}^{\mathrm{peak}} \cong \omega_{ij}\left[1 - \frac{1}{8}\left(\frac{\Gamma_{ij}}{\omega_{ij}}\right)^2\right], \quad \Gamma_{ij} \ll \omega_{ij} \quad (29)$$

Equation 28 or 29 represents a spectral red shift or the Stokes spectroscopy. Equations 28 and 29 show us a way of estimating the transition eigenfrequency ω_{ij} of a hydrogen-like atom according to the peak frequency $\omega_{ij}^{\mathrm{peak}}$ and the FWHM Γ_{ij} of a material spectrum. By using eqs 2, 6, 8, and 1PA or 2PA selection rules of quantum mechanics, i.e., $\Delta l = \pm 1$ for 1PA or $\Delta l = 0, \pm 2$ for 2PA, where $l = j - j_\varphi$ corresponding to s, p, d, f··· orbits for $j_\varphi = j, j-1, j-2, \cdots$ respectively, one can obtain the effective quantum numbers before and after the electronic transitions of the 1PA or 2PA process.

For the second-order susceptibility of a medium, we have

$$\chi^{(2)}(\omega_1, \omega_2) = \frac{e^3}{\varepsilon_0 m^2} \sum_i \sum_{j>i} (-A_j) N'_{i\to j} F_{ij}(\omega_1 + \omega_2) F_{ij}(\omega_1) F_{ij}(\omega_2) \quad (30)$$

When $\omega_1 = \omega_2 = \omega$, the real and imaginary parts of $\chi^{(2)}(\omega, \omega)$ are, respectively,

https://doi.org/10.1021/acsomega.3c01922
ACS Omega 2023, 8, 19950−19962

$$\chi_{\mathrm{Re}}^{(2)}(\omega,\omega)=\sum_i\sum_{j>i}[\chi_{ij}^{(2)}(\omega,\omega)]_{\mathrm{Re}}$$
$$=\frac{e^3}{\varepsilon_0 m^2}\sum_i\sum_{j>i}\frac{(-A_j)N'_{i\to j}}{\omega_{ij}^6}$$
$$\left\{\frac{\left(1-\frac{4\omega^2}{\omega_{ij}^2}\right)\left[\left(1-\frac{\omega^2}{\omega_{ij}^2}\right)^2-\frac{\Gamma_{ij}^2\omega^2}{\omega_{ij}^4}\right]-\frac{4\Gamma_{ij}^2\omega^2}{\omega_{ij}^4}\left(1-\frac{\omega^2}{\omega_{ij}^2}\right)}{\left[\left(1-\frac{4\omega^2}{\omega_{ij}^2}\right)^2+\frac{4\Gamma_{ij}^2\omega^2}{\omega_{ij}^4}\right]\times\left[\left(1-\frac{\omega^2}{\omega_{ij}^2}\right)^2+\frac{\Gamma_{ij}^2\omega^2}{\omega_{ij}^4}\right]^2}\right\} \quad (31)$$

and

$$\chi_{\mathrm{Im}}^{(2)}(\omega,\omega)=\sum_i\sum_{j>i}[\chi_{ij}^{(2)}(\omega,\omega)]_{\mathrm{Im}}$$
$$=\frac{e^3}{\varepsilon_0 m^2}\sum_i\sum_{j>i}\frac{(-A_j)N'_{i\to j}}{\omega_{ij}^6}$$
$$\frac{\frac{2\Gamma_{ij}\omega}{\omega_{ij}^2}\left\{\left(1-\frac{4\omega^2}{\omega_{ij}^2}\right)\left(1-\frac{\omega^2}{\omega_{ij}^2}\right)+\left[\left(1-\frac{\omega^2}{\omega_{ij}^2}\right)^2-\frac{\Gamma_{ij}^2\omega^2}{\omega_{ij}^4}\right]\right\}}{\left[\left(1-\frac{4\omega^2}{\omega_{ij}^2}\right)^2+\frac{4\Gamma_{ij}^2\omega^2}{\omega_{ij}^4}\right]\times\left[\left(1-\frac{\omega^2}{\omega_{ij}^2}\right)^2+\frac{\Gamma_{ij}^2\omega^2}{\omega_{ij}^4}\right]^2} \quad (32)$$

For the third-order susceptibility relating to the third harmonic generation (THG), we have

$$\chi^{(3)}(\omega_1,\omega_2,\omega_3)=\frac{e^4}{\varepsilon_0 m^3}\sum_i\sum_{j>i}N'_{i\to j}$$
$$\left\{\frac{2}{3}A_j^2[F_{ij}(\omega_1+\omega_2)+F_{ij}(\omega_2+\omega_3)+F_{ij}(\omega_3+\omega_1)]-B_j\right\}\times F_{ij}(\omega_1+\omega_2+\omega_3)F_{ij}(\omega_1)F_{ij}(\omega_2)F_{ij}(\omega_3) \quad (33)$$

When $\omega_1=\omega_2=\omega_3=\omega$

$$\chi^{(3)}(\omega,\omega,\omega)=\frac{e^4}{\varepsilon_0 m^3}\sum_i\sum_{j>i}N'_{i\to j}\{2A_j^2F_{ij}(2\omega)-B_j\}F_{ij}(3\omega)F_{ij}^3(\omega) \quad (34)$$

The real and imaginary parts of $\chi^{(3)}(\omega,\omega,\omega)$ are, respectively,

$$\chi_{\mathrm{Re}}^{(3)}(\omega,\omega,\omega)=\frac{e^4}{\varepsilon_0 m^3}\sum_i\sum_{j>i}\frac{N'_{i\to j}}{\omega_{ij}^8}\times\left\{\left[\frac{\frac{2A_j^2}{\omega_{ij}^2}\left(1-\frac{4\omega^2}{\omega_{ij}^2}\right)}{\left(1-\frac{4\omega^2}{\omega_{ij}^2}\right)^2+\frac{4\Gamma_{ij}^2\omega^2}{\omega_{ij}^4}}-B_j\right]\left\{\left(1-\frac{9\omega^2}{\omega_{ij}^2}\right)\left[\left(1-\frac{\omega^2}{\omega_{ij}^2}\right)^3-\frac{3\Gamma_{ij}^2\omega^2}{\omega_{ij}^4}\left(1-\frac{\omega^2}{\omega_{ij}^2}\right)\right]\right.\right.$$
$$\left.\left.-\frac{3\Gamma_{ij}\omega}{\omega_{ij}^2}\left[\frac{3\Gamma_{ij}\omega}{\omega_{ij}^2}\left(1-\frac{\omega^2}{\omega_{ij}^2}\right)^2-\frac{\Gamma_{ij}^3\omega^3}{\omega_{ij}^6}\right]\right\}\Bigg/\left\{\left[\left(1-\frac{\omega^2}{\omega_{ij}^2}\right)^2+\frac{\Gamma_{ij}^2\omega^2}{\omega_{ij}^4}\right]^3\left[\left(1-\frac{9\omega^2}{\omega_{ij}^2}\right)^2+\frac{9\Gamma_{ij}^2\omega^2}{\omega_{ij}^4}\right]\right\}$$
$$-\frac{\frac{4A_j^2\Gamma_{ij}\omega}{\omega_{ij}^4}}{\left(1-\frac{4\omega^2}{\omega_{ij}^2}\right)^2+\frac{4\Gamma_{ij}^2\omega^2}{\omega_{ij}^4}}\left\{\left(1-\frac{9\omega^2}{\omega_{ij}^2}\right)\left[\frac{3\Gamma_{ij}\omega}{\omega_{ij}^2}\left(1-\frac{\omega^2}{\omega_{ij}^2}\right)^2-\frac{\Gamma_{ij}^3\omega^3}{\omega_{ij}^6}\right]+\frac{3\Gamma_{ij}\omega}{\omega_{ij}^2}\left[\left(1-\frac{\omega^2}{\omega_{ij}^2}\right)^3-\frac{3\Gamma_{ij}^2\omega^2}{\omega_{ij}^4}\left(1-\frac{\omega^2}{\omega_{ij}^2}\right)\right]\right\}$$
$$\Bigg/\left\{\left[\left(1-\frac{\omega^2}{\omega_{ij}^2}\right)^2+\frac{\Gamma_{ij}^2\omega^2}{\omega_{ij}^4}\right]^3\left[\left(1-\frac{9\omega^2}{\omega_{ij}^2}\right)^2+\frac{9\Gamma_{ij}^2\omega^2}{\omega_{ij}^4}\right]\right\}\Bigg\} \quad (35)$$

https://doi.org/10.1021/acsomega.3c01922
ACS Omega 2023, 8, 19950−19962

$$\chi^{(3)}_{\mathrm{Im}}(\omega,\omega,\omega)=\frac{e^4}{\varepsilon_0 m^3}\sum_i\sum_{j>i}\frac{N'_{i\to j}}{\omega_{ij}^8}\times\left\{\left[\frac{\frac{2A_j^2}{\omega_{ij}^2}\left(1-\frac{4\omega^2}{\omega_{ij}^2}\right)}{\left(1-\frac{4\omega^2}{\omega_{ij}^2}\right)^2+\frac{4\Gamma_{ij}^2\omega^2}{\omega_{ij}^4}}-B_j\right]\left\{\left(1-\frac{9\omega^2}{\omega_{ij}^2}\right)\left[\frac{3\Gamma_{ij}\omega}{\omega_{ij}^2}\left(1-\frac{\omega^2}{\omega_{ij}^2}\right)^2-\frac{\Gamma_{ij}^3\omega^3}{\omega_{ij}^6}\right]\right.\right.$$
$$\left.\left.+\frac{3\Gamma_{ij}\omega}{\omega_{ij}^2}\left[\left(1-\frac{\omega^2}{\omega_{ij}^2}\right)^3-\frac{3\Gamma_{ij}^2\omega^2}{\omega_{ij}^4}\left(1-\frac{\omega^2}{\omega_{ij}^2}\right)\right]\right\}\Bigg/\left\{\left[\left(1-\frac{\omega^2}{\omega_{ij}^2}\right)^2+\frac{\Gamma_{ij}^2\omega^2}{\omega_{ij}^4}\right]^3\left[\left(1-\frac{9\omega^2}{\omega_{ij}^2}\right)^2+\frac{9\Gamma_{ij}^2\omega^2}{\omega_{ij}^4}\right]\right\}$$
$$+\frac{\frac{4A_j^2\Gamma_{ij}\omega}{\omega_{ij}^4}}{\left(1-\frac{4\omega^2}{\omega_{ij}^2}\right)^2+\frac{4\Gamma_{ij}^2\omega^2}{\omega_{ij}^4}}\left\{\left(1-\frac{9\omega^2}{\omega_{ij}^2}\right)\left[\left(1-\frac{\omega^2}{\omega_{ij}^2}\right)^3-\frac{3\Gamma_{ij}^2\omega^2}{\omega_{ij}^4}\left(1-\frac{\omega^2}{\omega_{ij}^2}\right)\right]-\frac{3\Gamma_{ij}\omega}{\omega_{ij}^2}\left[\frac{3\Gamma_{ij}\omega}{\omega_{ij}^2}\left(1-\frac{\omega^2}{\omega_{ij}^2}\right)^2-\frac{\Gamma_{ij}^3\omega^3}{\omega_{ij}^6}\right]\right\}$$
$$\Bigg/\left\{\left[\left(1-\frac{\omega^2}{\omega_{ij}^2}\right)^2+\frac{\Gamma_{ij}^2\omega^2}{\omega_{ij}^4}\right]^3\left[\left(1-\frac{9\omega^2}{\omega_{ij}^2}\right)^2+\frac{9\Gamma_{ij}^2\omega^2}{\omega_{ij}^4}\right]\right\} \tag{36}$$

For another third-order electric polarizability relating to 2PA and the nonlinear refractive index coefficient, we have

$$\chi^{(3)}(\omega,\omega,-\omega)=\frac{e^4}{3\varepsilon_0 m^3}\sum_i\sum_{j>i}N'_{i\to j}[2A_j^2F_{ij}(2\omega)+4A_j^2F_{ij}(0)-3B_j]F_{ij}^3(\omega)F_{ij}(-\omega) \tag{37}$$

The real and imaginary parts of $\chi^{(3)}(\omega,\omega,-\omega)$ are, respectively,

$$\chi^{(3)}_{\mathrm{Im}}(\omega,\omega,-\omega)=\sum_i\sum_{j>i}[\chi^{(3)}_{ij}(\omega,\omega,-\omega)]_{\mathrm{Im}}$$
$$=\frac{e^4}{3\varepsilon_0 m^3}\sum_i\sum_{j>i}\frac{N'_{i\to j}}{\omega_{ij}^8}\times\left\{\frac{\left[\frac{\frac{2A_j^2}{\omega_{ij}^2}\left(1-\frac{4\omega^2}{\omega_{ij}^2}\right)}{\left(1-\frac{4\omega^2}{\omega_{ij}^2}\right)^2+\left(\frac{\Gamma_{ij}2\omega}{\omega_{ij}^2}\right)^2}+\frac{4A_j^2}{\omega_{ij}^2}-3B_j\right]\frac{\Gamma_{ij}2\omega}{\omega_{ij}^2}\left(1-\frac{\omega^2}{\omega_{ij}^2}\right)}{\left[\left(1-\frac{\omega^2}{\omega_{ij}^2}\right)^2+\left(\frac{\Gamma_{ij}\omega}{\omega_{ij}^2}\right)^2\right]^3}\right.$$
$$\left.+\frac{\frac{4A_j^2}{\omega_{ij}^2}\frac{\Gamma_{ij}\omega}{\omega_{ij}^2}\left[\left(1-\frac{\omega^2}{\omega_{ij}^2}\right)^2-\left(\frac{\Gamma_{ij}\omega}{\omega_{ij}^2}\right)^2\right]}{\left[\left(1-\frac{4\omega^2}{\omega_{ij}^2}\right)^2+\left(\frac{\Gamma_{ij}2\omega}{\omega_{ij}^2}\right)^2\right]\left[\left(1-\frac{\omega^2}{\omega_{ij}^2}\right)^2+\left(\frac{\Gamma_{ij}\omega}{\omega_{ij}^2}\right)^2\right]^3}\right\} \tag{38}$$

$$\chi^{(3)}_{\mathrm{Re}}(\omega,\omega,-\omega)=\sum_i\sum_{j>i}[\chi^{(3)}_{ij}(\omega,\omega,-\omega)]_{\mathrm{Re}}$$
$$=\frac{e^4}{3\varepsilon_0 m^3}\sum_i\sum_{j>i}\frac{N'_{i\to j}}{\omega_{ij}^8}$$
$$\times\left\{\frac{\left[\frac{\frac{2A_j^2}{\omega_{ij}^2}\left(1-\frac{4\omega^2}{\omega_{ij}^2}\right)}{\left(1-\frac{4\omega^2}{\omega_{ij}^2}\right)^2+\left(\frac{\Gamma_{ij}2\omega}{\omega_{ij}^2}\right)^2}+\frac{4A_j^2}{\omega_{ij}^2}-3B_j\right]\left[\left(1-\frac{\omega^2}{\omega_{ij}^2}\right)^2-\left(\frac{\Gamma_{ij}\omega}{\omega_{ij}^2}\right)^2\right]}{\left[\left(1-\frac{\omega^2}{\omega_{ij}^2}\right)^2+\left(\frac{\Gamma_{ij}\omega}{\omega_{ij}^2}\right)^2\right]^3}\right.$$
$$\left.-\frac{\frac{8A_j^2}{\omega_{ij}^2}\left(1-\frac{\omega^2}{\omega_{ij}^2}\right)\left(\frac{\Gamma_{ij}\omega}{\omega_{ij}^2}\right)^2}{\left[\left(1-\frac{4\omega^2}{\omega_{ij}^2}\right)^2+\left(\frac{2\Gamma_{ij}\omega}{\omega_{ij}^2}\right)^2\right]\left[\left(1-\frac{\omega^2}{\omega_{ij}^2}\right)^2+\left(\frac{\Gamma_{ij}\omega}{\omega_{ij}^2}\right)^2\right]^3}\right\} \tag{39}$$

Table 1. 2PA Cross-Section Deviations between the Experimental Result and the QILO's One

organic molecules	$\sigma_{\max}$ (experiment) (GM)	$\sigma_{\max}$ (theory) (GM)	deviation (%)
LB3	2250 (850 nm)	2228 (850 nm)	−0.9
M4	726 (851 nm)	793 (851 nm)	10

For the 2PA transition process, the molecular 2PA cross section can be given by eq 40

https://doi.org/10.1021/acsomega.3c01922
ACS Omega 2023, 8, 19950−19962

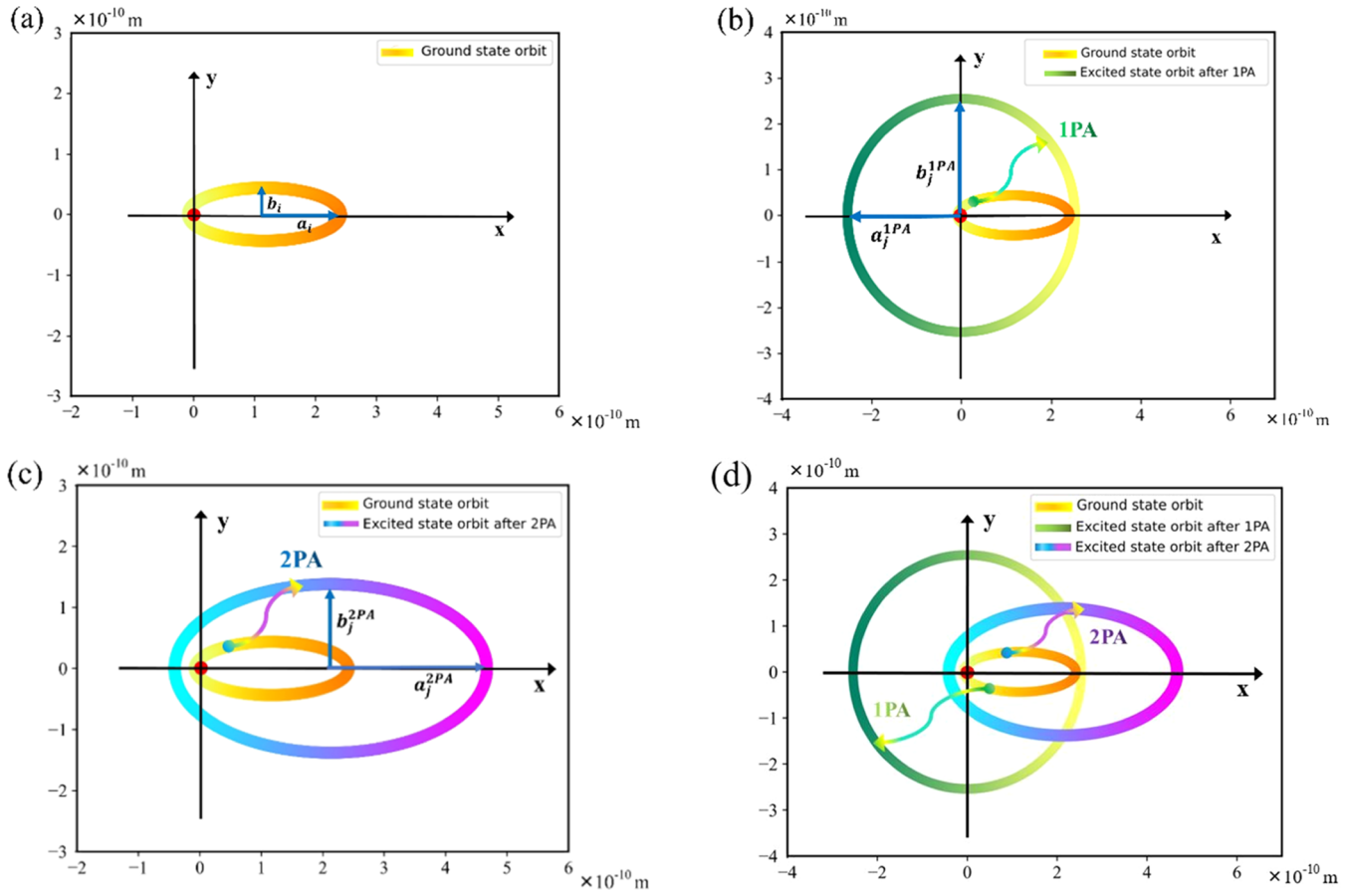

Figure 4. Charge-transfer images in 1PA and 2PA processes of the compound LB3 in THF. (a) Ground state i = 1.5367, i_φ = i-1 = 0.5367, a_i = 1.2492 Å, b_i = 0.4363 Å, and μ_i = 5.6145 D. (b) Final state after 1PA j = 2.1912, j_φ = j = 2.1912, and a_j = b_j = 2.5399 Å. (c) Final state after 2PA j = 2.1912, j_φ = j-1 = 1.1912, a_j = 2.5399 Å b_j = 1.3808 Å, and μ_j = 10.2256 D. (d) Comparison of the CT orbits between 1PA and 2PA transitions.

$$\sigma_2 = \frac{2\hbar e^4}{3\varepsilon_0 c^2 n_{\mathrm{Re}}^2 m^3} \sum_i \sum_{j>i} \frac{\omega^2}{\omega_{ij}^8} \times \left\{ \frac{\left[\frac{\frac{2A_j^2}{\omega_{ij}^2}\left(1-\frac{4\omega^2}{\omega_{ij}^2}\right)}{\left(1-\frac{4\omega^2}{\omega_{ij}^2}\right)^2+\left(\frac{\Gamma_{ij}2\omega}{\omega_{ij}^2}\right)^2} + \frac{4A_j^2}{\omega_{ij}^2} - 3B_j \right] \frac{\Gamma_{ij}2\omega}{\omega_{ij}^2}\left(1-\frac{\omega^2}{\omega_{ij}^2}\right)}{\left[\left(1-\frac{\omega^2}{\omega_{ij}^2}\right)^2+\left(\frac{\Gamma_{ij}\omega}{\omega_{ij}^2}\right)^2\right]^3} + \frac{\frac{4A_j^2}{\omega_{ij}^2}\frac{\Gamma_{ij}\omega}{\omega_{ij}^2}\left[\left(1-\frac{\omega^2}{\omega_{ij}^2}\right)^2-\left(\frac{\Gamma_{ij}\omega}{\omega_{ij}^2}\right)^2\right]}{\left[\left(1-\frac{4\omega^2}{\omega_{ij}^2}\right)^2+\left(\frac{\Gamma_{ij}2\omega}{\omega_{ij}^2}\right)^2\right]\left[\left(1-\frac{\omega^2}{\omega_{ij}^2}\right)^2+\left(\frac{\Gamma_{ij}\omega}{\omega_{ij}^2}\right)^2\right]^3} \right\} \quad (40)$$

By means of the above equations, we have investigated a charge-transfer image in molecular photon-absorption via numerical simulations of 1PA and 2PA behaviors of the two organic molecule compounds. We have also calculated the energy level lifetime of the compounds. Some detailed results are as follows.

3. RESULTS AND DISCUSSION

Cai et al.[40] designed and synthesized many organic molecules with the purpose of obtaining a large molecular 2PA cross section, one of which is LB3, as shown in Figure 3. The black solid line in Figure 3b represents the linear absorptive spectrum of LB3. Through fitting the absorptive spectrum of LB3 as is shown by the red solid line in Figure 3c using the QILO model, we can obtain the damping coefficient $\Gamma_{ij} \approx 6.25 \times 10^{14}$ s^{-1} near the absorptive peak wavelength 425 nm corresponding to the peak angular frequency $\omega_{ij}^{\mathrm{peak}} = 4.4329 \times 10^{15}$ rad·s^{-1}. Taking the values of Γ_{ij} and $\omega_{ij}^{\mathrm{peak}}$ into eq 29, we can obtain the angular eigenfrequency $\omega_{ij} = 4.4439 \times 10^{15}$ rad·s^{-1} (λ_{ij} = 423.9 nm) of the 1PA jumping process of the LB3 molecule around the spectral peak wavelength. Considering that LB3 is a polar molecule in the ground state and given the 1PA selection rules of quantum

Table 2. Level Lifetimes of LB3 and M4 in, respectively, 1PA and 2PA Processes

organic molecules	$\tau_{ij}^{1\mathrm{PA}}$ (ps)	$\tau_{ij}^{2\mathrm{PA}}$ (ps)	relative difference (%)
LB3	32.6	16.5	49
M4	37.4	19.8	47

https://doi.org/10.1021/acsomega.3c01922
ACS Omega 2023, 8, 19950−19962

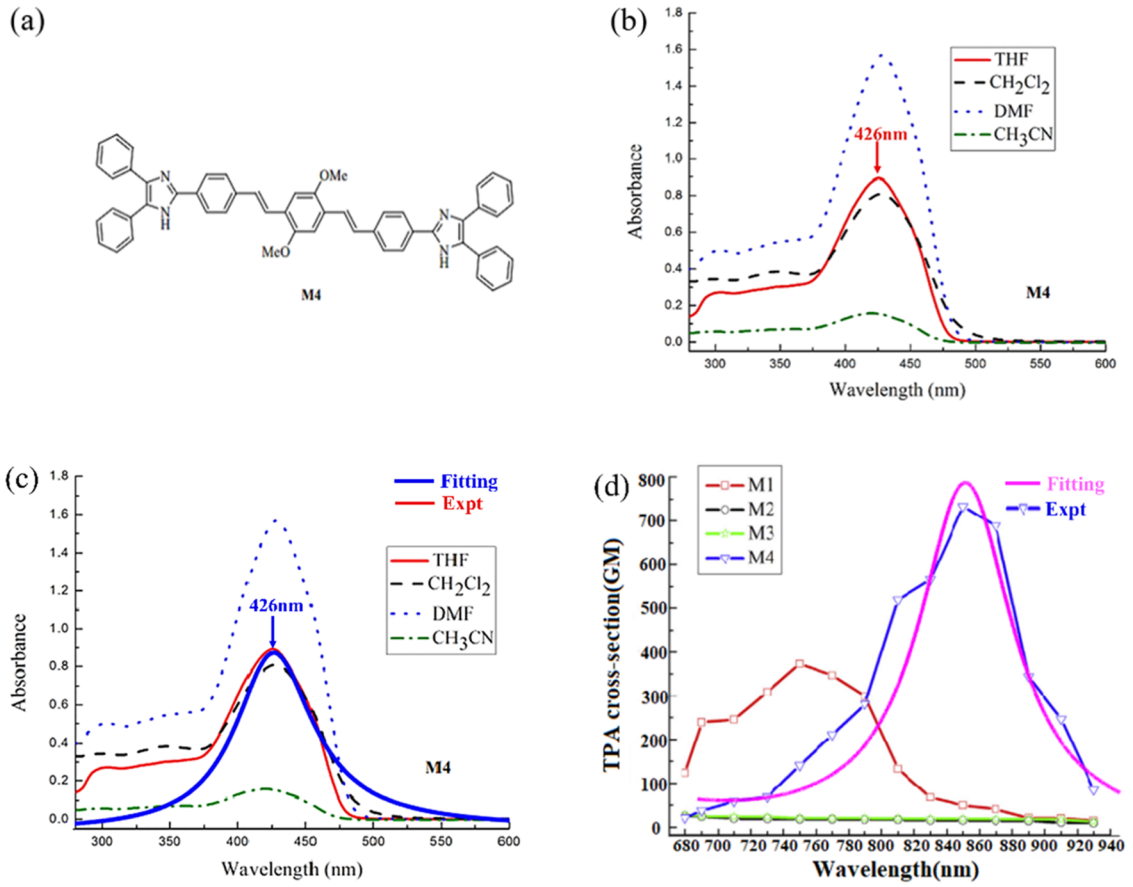

Figure 5. Experimental 1PA and 2PA of M4 and theoretical simulations based on the QILO model. (a) Molecular structure, (b) 1PA spectrum,[47] (c) fitting diagram (blue line) of the 1PA spectrum using QILO, and (d) experimental 2PA cross section and its numerical simulation using the QILO model (purple line).

mechanics $\Delta l = \pm 1$, we believe that the black line of the 1PA spectrum near 425 nm in Figure 3b represents the 2p → 3s transition process of the molecule. Using $\Gamma_{ij} = 6.25 \times 10^{14}$ s^{-1}, $\omega_{ij} = 4.4439 \times 10^{15}$ rad·s^{-1}, $i_\varphi = i$-1, and $j_\varphi = j$ in eq 2 and eq 8, we can obtain the effective quantum numbers before and after the electronic transitions, respectively, as $i = 1.5367$, $i_\varphi = 0.5367$, $j = 2.1912$, and $j_\varphi = j = 2.1912$ for the eigenfrequency $\omega_{ij} = 4.4439 \times 10^{15}$ rad·s^{-1} of LB3. According to the transition selection rule $\Delta l = 0$ for 2PA, the effective quantum numbers before and after the electronic transitions of LB3 are, respectively, $i = 1.5367$, $i_\varphi = 0.5367$, $j = 2.1912$, and $j_\varphi = 1.1912$ (= j-1) corresponding to the 2p → 3p for the 2PA transition process, in which the damping coefficient $\Gamma^{2PA} = 3.1685 \times 10^{14}$ s^{-1} around the wavelength 850 nm. In eq 8, the effective radius of the THF solvent molecule $R' = 3.0229$ Å relating to the molecular number density $N' = 7.4168 \times 10^{27}$ m^{-3}, where the adjustable constant $\delta = 0.96$. According to eqs 11−14, we can obtain the second- and third-order nonlinear effect parameters $A_{2.1912} = 5.8430 \times 10^{41}$ SI and $B_{2.1912} = 1.0115 \times 10^{51}$ SI. Using eq 40, we have calculated the 2PA cross section of LB3 as shown in Figure 3d (green line). Figure 3d exhibits that the theoretical 2PA cross section of LB3 inferred by the QILO model turns out to be in good agreement with the experimental one. The 2PA cross-section deviation between the measured result and QILO's one at the peak wavelength of 850 nm is only about −1.0%, as shown in Table 1. It needs to be explained that the most important factor influencing the error is the damping coefficient or FWHM Γ_{ij} of the linear absorption spectrum.

Substituting the effective quantum numbers $i = 1.5367$ and $i_\varphi = 0.5367$ in the 1PA process near the peak wavelength 425 nm into eqs 4, 5, and 16, we can obtain that the semimajor axis, the semiminor axis, and the average electric dipole moment of the LB3 molecule in the ground-state orbit are, respectively, $a_i = 1.2492 \times 10^{-10}$ m = 1.2492 Å, $b_i = 0.4363$ Å, and $\mu_i = 1.8728 \times 10^{-29}$ C·m = 5.6145 D, as shown in Figure 4a. For the 1PA process, in a similar manner, using $j = 2.1912$ and $j_\varphi = j = 2.1912$ in eqs 4, 5, and 16, we can obtain that the semimajor axis, the semiminor axis, and the average electric dipole moment of the LB3 molecule at the related excited-state orbit are, respectively, $a_j = 2.5399$ Å, semiminor axis $b_j = a_j$, and $\mu_j = 0$, as shown in Figure 4b. In the 2PA transition process near the wavelength 850 nm, using the effective quantum numbers $j = 2.1912$ and $j_\varphi = j$-1 = 1.1912 in eq 4, 5, and 16, we can obtain that the semimajor axis $a_j = 2.5399$ Å, the semiminor axis $b_j = 1.3808$ Å, and the average electric dipole moment $\mu_j = 3.4109 \times 10^{-29}$ C·m = 10.2256 D of the LB3 molecule in THF at the two-photon-excited j state orbit as shown in Figure 4c.

Figure 4c indicates that, through the 2-photon-absorption process, a great change of the molecular dipole moment of LB3 from the ground state to the excited state has taken place. This result is in keeping with the general conclusion of the great increase of the molecular dipole moment from the ground state to the excited state by two-photon excitation

https://doi.org/10.1021/acsomega.3c01922
ACS Omega 2023, 8, 19950−19962

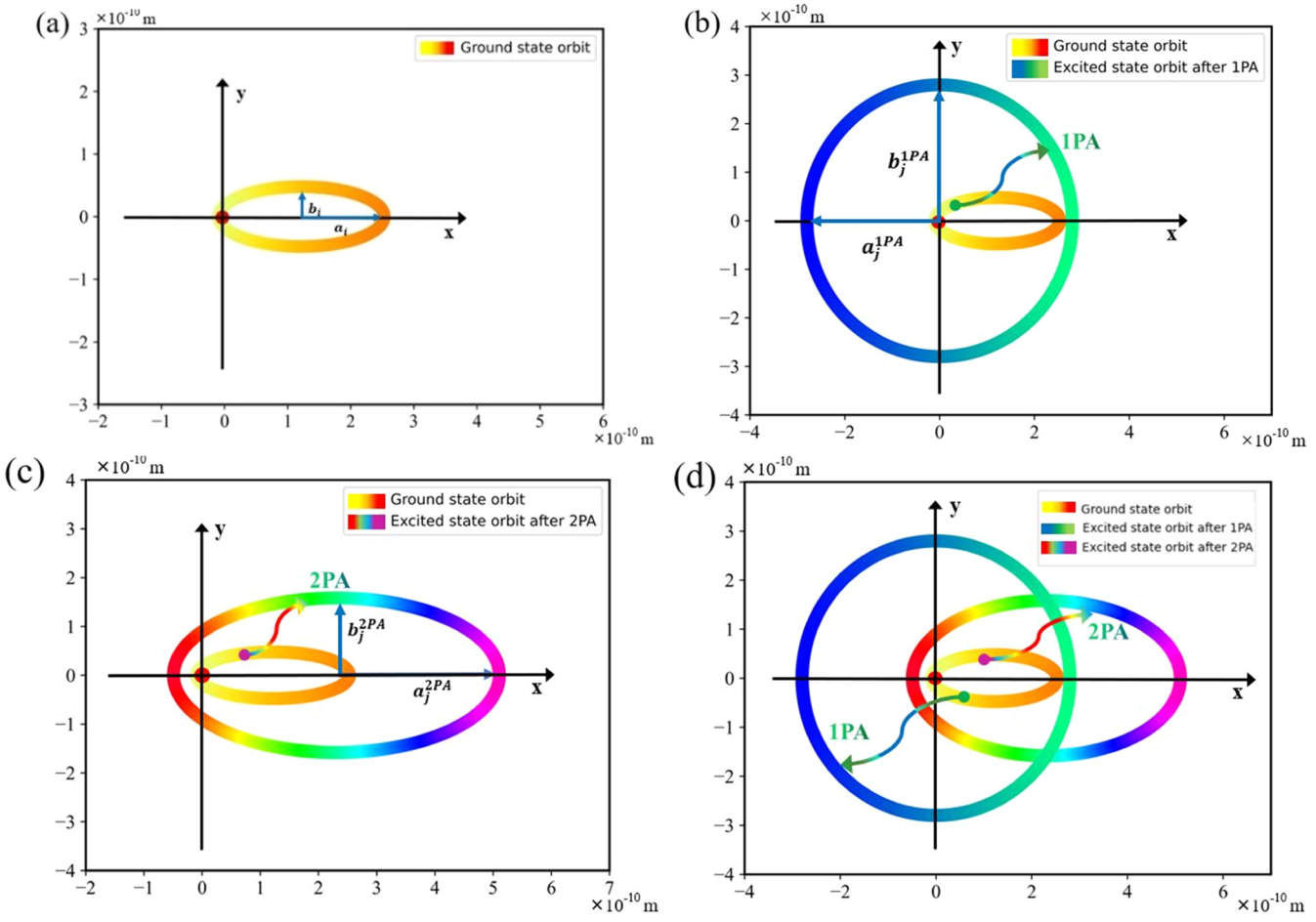

Figure 6. Charge-transfer images in 1PA and 2PA processes of the compound M4 in THF. (a) Ground state i = 1.5740, i_φ = i-1 = 0.5740, a_i = 1.3106 Å, b_i = 0.4779 Å, and μ_i = 5.8540 D; (b) final state after 1PA j = 2.3001, j_φ = j = 2.3001, and a_j = b_j = 2.7987 Å; (c) final state after 2PA j = 2.3001, j_φ = j-1 = 1.3001, a_j = 2.7987 Å b_j = 1.5819 Å, and μ_j = 11.0742 D; (d) comparison of the CT orbits between 1PA and 2PA transitions.

according to the time-dependent density functional theory (TDDFT) in the literature.[26,41,42] The compared final-state orbits of LB3 between the 1PA transition near 425 nm and the 2PA transition near 850 nm are exhibited in Figure 4d. Figure 4 shows our abridged general view of the charge-transfer images in molecular 1PA and 2PA processes of the compound LB3 in the THF solvent on the basis of the QILO model.

The measurement of an excited-state lifetime is nowadays a relatively mature technology. Considering the QILO model, the energy level lifetime is likely to provide valuable insights into the comprehension of the CT image. For the convenience of comparison in energy level lifetime calculations, we chose the LB3 sample concentration in the 1PA process to be the same as the one in the 2PA process. For the sample concentration C_0 = 1.0 × 10^{-5} mol/L, we can obtain the number density of transition electrons of LB3 molecules to be about N_{ij} = 6.022 × 10^{21} m^{-3} in eq 20. Here, we assume that only the outermost one electron of a hydrogen-like atom of LB3 is excited under a light field. Using Γ_{ij} = 6.25 × 10^{14} s^{-1} near the absorptive peak wavelength 425 nm for 1PA and Γ^{2PA} = 3.1685 × 10^{14} s^{-1} around the wavelength 850 nm for 2PA in eq 20, we can obtain the excited-state lifetimes of LB3 molecules, respectively, through 1PA and 2PA excitations as shown in Table 2. The calculated level lifetimes based on eq 20 are the same order of magnitude (ps or ns) as the experimental ones.[43−46] Table 2 indicates that there is a big difference in the level lifetimes between the two kinds of excitations (1PA and 2PA) for a given sample. Considering the QILO model, this difference should be owing to the different transition selection rules of 1PA and 2PA in quantum mechanics. This result may suggest that, by means of level-lifetime measurement, perhaps one can test indirectly the transition selection rule of quantum mechanics, which is a result of the pure theoretical analysis of the frontier orbit symmetry in single- and two-photon processes.

Using the same method as for the compound LB3, we have also investigated the detailed behaviors of another polar molecule M4 as shown in Figure 5a in the THF solvent, such as the effective quantum numbers before and after the electronic transitions near the 1PA and 2PA peak wavelengths, the molecular 2PA cross section, the Bohr−Sommerfeld orbits of initial and final states, the excited-state lifetime, and so on. The obtained results are, respectively, indicated in Figures 5 and 6 and Tables 1 and 2. These results indicate that the optoelectronic behaviors of the compound M4 are similar to the ones of LB3 in the same solvent.

https://doi.org/10.1021/acsomega.3c01922
ACS Omega 2023, 8, 19950−19962

As is known to all, the molecular spectrum is related to the effect of the solvent. The effect can be shown partly through the peak frequency and FWHM of an absorptive spectrum. Since the effective quantum numbers before and after the electronic transitions come from the solutions of eqs 2, 8, and 29, the CT process of QILO could be used to explain some results of the solvent effect in part. Furthermore, our results indicate that the molecular charge transfer and level lifetime in 1PA are obviously different from the ones in 2PA. This result suggests that the QILO model might be helpful in dealing with the structural design and synthetic strategies of intramolecular charge-transfer compounds as well as their potential applications by means of 1PA or 2PA excitation.[48−52]

Besides the charge transfer and level lifetime in molecular photon-absorption, we have investigated in detail the nonlinear refractive index coefficient and the second or third harmonic properties of some photoelectric materials on the basis of the QILO model as well. Some expected results have been obtained. The relevant research are in progress.

4. CONCLUSIONS

In summary, the quantum impedance Lorentz oscillator (QILO) model provides us with such a charge-transfer image in the molecular single-photon- or multiphoton-absorption process that a hydrogen-like atomic electron of a molecule transits among the different Bohr−Sommerfeld orbits that are required to satisfy simultaneously the conditions of the transition selection rules of quantum mechanics. It would make the estimation of a molecular average dipole moment very easy and simple. In addition, the level-lifetime formula based on the microparticle collision idea of thermal motion might offer a practical method to theoretically estimate the excited-state lifetime in the electronic transition process between two different energy levels. It may be helpful to deal with material spectral behaviors measured in room-temperature conditions. Our result suggests that the level lifetime of QILO may be used for an experimental method to verify 1PA and 2PA transition selection rules resulting from the pure theoretical analysis of frontier orbit symmetry in quantum mechanics. The QILO model exhibits the advantage of simplifying the calculation complexity and reducing the high cost associated with the first principle in addressing both linear and nonlinear properties of optoelectronic materials.

AUTHOR INFORMATION

Corresponding Authors

Yong Zhang − *School of Science, Hebei University of Technology, Tianjin 300401, China; Hebei Key Laboratory of Advanced Laser Technology and Equipment, Tianjin 300401, China*; Email: 13902109749@163.com

Xing-Hua Zhao − *School of Science, Hebei University of Technology, Tianjin 300401, China*; Email: zxh@hebut.edu.cn

Pei-De Zhao − *School of Science, Hebei University of Technology, Tianjin 300401, China; Hebei Key Laboratory of Advanced Laser Technology and Equipment, Tianjin 300401, China*; Email: pdzhao@hebut.edu.cn, pdzhao@eyou.com

Authors

Qi-Qi Bai − *School of Science, Hebei University of Technology, Tianjin 300401, China*; orcid.org/0009-0004-5253-8408

Zheng-Ji Fang − *School of Science, Hebei University of Technology, Tianjin 300401, China*

Xiao-Feng Wang − *School of Science, Hebei University of Technology, Tianjin 300401, China*

Complete contact information is available at: https://pubs.acs.org/10.1021/acsomega.3c01922

Funding

This work was supported by the Natural Science Foundation of Hebei Province (No. F2021202002), the National Natural Science Foundation of China (Grant No. 62005074).

Notes

The authors declare no competing financial interest.

REFERENCES

(1) Johnson, K.; Huang, Y.-S.; Huettner, S.; Sommer, M.; Brinkmann, M.; Mulherin, R.; Niedzialek, D.; Beljonne, D.; Clark, J.; Huck, W. T. S.; Friend, R. H. Control of Intrachain Charge Transfer in Model Systems for Block Copolymer Photovoltaic Materials. *J. Am. Chem. Soc.* **2013**, *135*, 5074−5083.

(2) Jakowetz, A. C.; Böhm, M. L.; Zhang, J.; Sadhanala, A.; Huettner, S.; Bakulin, A. A.; Rao, A.; Friend, R. H. What Controls the Rate of Ultrafast Charge Transfer and Charge Separation Efficiency in Organic Photovoltaic Blends. *J. Am. Chem. Soc.* **2016**, *138*, 11672−11679.

(3) Ratchford, D. C. Plasmon-Induced Charge Transfer: Challenges and Outlook. *ACS Nano* **2019**, *13*, 13610−13614.

(4) Zamborlini, G.; Lüftner, D.; Feng, Z.; Kollmann, B.; Puschnig, P.; Dri, C.; Panighel, M.; Santo, G. D.; Goldoni, A.; Comelli, G.; Jugovac, M.; Feyer, V.; Schneider, C. M. Multi-orbital charge transfer at highly oriented organic/metal interfaces. *Nat. Commun.* **2017**, *8*, No. 335.

(5) Gera, R.; Dasgupta, J. Photochemistry using a host−guest charge transfer paradigm: DMABN as a dynamical probe of ground and excited states. *Phys. Chem. Chem. Phys.* **2021**, *23*, 9280−9284.

(6) London, H. C.; Whittemore, T. J.; Gale, A. G.; McMillen, C. D.; Pritchett, D. Y.; Myers, H. D.; Thomas, G. C.; Shields, G. C.; Wagenknecht, P. S. Ligand-to-Metal Charge-Transfer Photophysics and Photochemistry of Emissive d^0 Titanocenes: A Spectroscopic and Computational Investigation. *Inorg. Chem.* **2021**, *60*, 14399−14409.

(7) Fecková, M.; Kalis, I. K.; Roisnel, T.; Poul, P. L.; Pytela, O.; Klikar, M.; Fakis, M.; Bureš, F. Photophysics of 9, 9-Dimethylacridan-Substituted Phenylstyrylpyrimidines Exhibiting Long-Lived Intramolecular Charge-Transfer Fluorescence and Aggregation-Induced Emission Characteristics. *Chem. - Eur. J.* **2021**, *27*, 1145−1159.

(8) Yang, S.; Cao, C.; Li, J. Y.; Deng, Z. Q.; Ni, S. F.; Jian, J. X.; Tong, Q. X.; Dang, L.; Li, M. D. Unveiling the π-Chain Effect on Charge Transfer and Charge Recombination Among Donor- π-Acceptor Material Systems. *J. Phys. Chem. C* **2022**, *126*, 1076−1084.

(9) Bendix, J.; Bechgaard, K.; Christensen, J. B. A new donor for charge-transfer systems: synthesis and properties of 2, 4, 7, 9-tetramethyl-1,6-dithiapyrene(TMDTP)and structure of $(TMDTP)_3(PF6)_2{\cdot}2THF$ and TMDTP−TCNQ. *RSC Adv.* **2021**, *11*, 14607−14614.

(10) Zong, H.; Wang, X.; Quan, J.; Tian, C. H.; Sun, M. T. Photoinduced charge transfer by one and two-photon absorptions: Physical mechanisms and applications. *Phys. Chem. Chem. Phys.* **2018**, *20*, 19720−19743.

(11) Lu, C.; Chen, X. Nanostructure engineering of graphitic carbon nitride for electrochemical applications. *ACS Nano* **2021**, *15*, 18777−18793.

(12) Reddy, K. A. J.; Reddy, D. A.; Hong, D. H.; Gopannagari, M.; Rangappa, A. P.; Kumar, D. P.; Kim, T. K. Impact of the number of surface-attached tungsten diselenide layers on cadmium sulfide nanorods on the charge transfer and photocatalytic hydrogen evolution rate. *J. Colloid Interface Sci.* **2022**, *608*, 903−911.
(13) Yamane, M.; Kanzaki, Y.; Mitsunuma, H.; Motomu, K. Titanium (IV) Chloride-Catalyzed Photoalkylation via C (sp3)−H Bond Activation of Alkanes. *Org. Lett.* **2022**, *24*, 1486−1490.
(14) Patnaik, S.; Mishra, B. P.; Parida, K. A review on dimensionally controlled synthesis of gC 3 N 4 and formation of an isotype heterojunction for photocatalytic hydrogen evolution. *Catal. Sci. Technol.* **2021**, *11*, 7505−7524.
(15) Elg, D. T.; Delgado, H. E.; Martin, D. C.; Sankaran, R. M.; Rumbach, P.; Bartels, D. M.; Go, D. B. Recent advances in understanding the role of solvated electrons at the plasma-liquid interface of solution-based gas discharges. *Spectrochim. Acta, Part B* **2021**, *186*, No. 106307.
(16) Hagstrum, H. D. Theory of Auger ejection of electrons from metals by ions. *Phys. Rev.* **1954**, *96*, 336−365.
(17) Shao, Y.; Lu, T.; Li, M.; Lu, W. Theoretical exploration of diverse electron-deficient core and terminal groups in A−DA′ D−A type non-fullerene acceptors for organic solar cells. *New J. Chem.* **2022**, *46*, 3370−3382.
(18) Los, J.; Geerlings, J. J. C. Charge exchange in atom-surface collisions. *Phys. Rep.* **1990**, *190*, 133−190.
(19) Gauyacq, J. P.; Borisov, A. G. Charge transfer in atom-surface collisions: effect of the presence of adsorbates on the surface. *J. Phys.: Condens. Matter* **1998**, *10*, 6585−6619.
(20) Valeri, S. Auger electron emission by ion impact on solid surfaces. *Surf. Sci. Rep.* **1993**, *17*, 85−150.
(21) Monreal, R. C. Auger neutralization and ionization processes for charge exchange between slow noble gas atoms and solid surfaces. *Prog. Surf. Sci.* **2014**, *89*, 80−125.
(22) Li, Y.; Liu, S.; Chen, M.; Ma, F. Photoinduced intermolecular and intramolecular charge transfer in the mixed coaggregates of pyrazoline and dicyanonaphthalene. *J. Photochem. Photobiol., A* **2009**, *205*, 139−144.
(23) Barrett, B. J.; Jimenez, D.; Klausen, R. S.; Bragg, A. E. Intramolecular Photoinduced Charge Transfer and Recombination Dynamics in Vinylarene Terminated Organosilanes. *J. Phys. Chem. B* **2021**, *125*, 8460−8471.
(24) Karatsu, T. Photochemistry and photophysics of organo-monosilane and oligosilanes: updating their studies on conformation and intramolecular interactions. *J. Photochem. Photobiol., C* **2008**, *9*, 111−137.
(25) Romero, A. H.; Romero, I. E.; Piro, O. E.; Echeverría, G. A.; Gotopo, L. A.; Moller, M. N.; Rodríguez, G. A.; Cabrera, G. J.; Castro, E. R.; López, S. E.; Cerecetto, H. E. Photo-induced partially aromatized intramolecular charge transfer. *J. Phys. Chem. B* **2021**, *125*, 9268−9285.
(26) Yu, L. B.; Hao, X. L.; Zhang, C.; He, T. F.; Ren, A. M. The theory of cysteine two-photon fluorescence probes of coumarino-coumarin derivatives and kinetics of ICT and PET mechanisms of probe molecules. *J. Photochem. Photobiol., A* **2020**, *397*, No. 112525.
(27) Zhang, M.; Zhang, M.; Zhao, G. Time-dependent density functional theory (TDDFT) study on the electronic spectroscopic blue-shift phenomenon and photoinduced charge transfer of firefly luciferin anion in aqueous solution: Insight into the excited-state hydrogen bond weakening mechanism. *J. Lumin.* **2018**, *195*, 116−119.
(28) Grabowski, Z. R.; Rotkiewicz, K.; Rettig, W. Structural changes accompanying intramolecular electron transfer: focus on twisted intramolecular charge-transfer states and structures. *Chem. Rev.* **2003**, *103*, 3899−4032.
(29) Sasaki, S.; Drummen, G. P. C.; Konishi, G. Recent advances in twisted intramolecular charge transfer (TICT) fluorescence and related phenomena in materials chemistry. *J. Mater. Chem. C* **2016**, *4*, 2731−2743.
(30) Zheng, J. J.; Sakaki, S. Molecule in Soft-Crystal at Ground and Excited States: Theoretical Approach. *J. Photochem. Photobiol., C* **2022**, *51*, No. 100482.
(31) Briggs, J. S.; Eisfeld, A. Quantum dynamics simulation with classical oscillators. *Phys. Rev. A* **2013**, *88*, No. 062104.
(32) Li, E. P.; Chu, H. S. *Plasmonic Nanoelectronics and Sensing*; Cambridge UniversityPress, 2014.
(33) Deymier, P. A.; Runge, K.; Vasseur, J. O. Geometric phase and topology of elastic oscillations and vibrations in model systems: Harmonic oscillator and superlattice. *AIP Adv.* **2016**, *6*, No. 121801.
(34) Martin, D. R.; Matyushov, D. V. Terahertz absorption of lysozyme in solution. *J. Chem. Phys.* **2017**, *147*, No. 084502.
(35) Berte, R.; Gubbin, C. R.; Wheeler, V. D.; Giles, A. J.; Giannini, V.; Maier, S. A.; Maier, S. A.; Caldwell, J. D. Sub-nanometer thin oxide film sensing with localized surface phonon polaritons. *ACS Photonics* **2018**, *5*, 2807−2815.
(36) Chen, S.; Kühne, P.; Stanishev, V.; Knight, S.; Brooke, R.; Petsagkourakis, I.; Crispin, X.; Schubert, M.; Darakchieva, V.; Jonsson, M. P. On the anomalous optical conductivity dispersion of electrically conducting polymers: ultra-wide spectral range ellipsometry combined with a Drude−Lorentz model. *J. Mater. Chem. C* **2019**, *7*, 4350−4362.
(37) Zhang, J.; Li, K.; Fang, Z. J.; Li, J.; Li, Q. Y.; Li, X. Q.; Zheng, Y.; Peng, Y. T.; Zhang, Y.; Zhao, P. D. Quantum impedance Lorentz oscillator and its 1-and 2-photon-absorption applications. *AIP Adv.* **2021**, *11*, No. 075218.
(38) Zhu, J.; Zhang, J.; Li, Y.; Zhang, Y.; Fang, Z. J.; Zhao, P. D.; Li, E. Quantized impedance dealing with the damping behavior of the one-dimensional oscillator. *AIP Adv.* **2015**, *5*, No. 117217.
(39) Daprà, M.; Niu, M. L.; Salumbides, E. J.; Murphy, M. T.; Ubachs, W. Constraint on a cosmological variation in the proton-to-electron mass ratio from electronic CO absorption. *Astrophys. J.* **2016**, *826*, No. 192.
(40) Cai, Z. B.; Shen, H. M.; Zhou, M.; Li, S. L.; Tian, Y. P. Novel A−(π−D−π−A) 1−3 branched fluorophores displaying high two-photon absorption. *RSC Adv.* **2016**, *6*, 46853−46863.
(41) Hong-Yu, L.; Ke, Z.; Rui-Qin, P.; Yuan-Hong, S.; Chuan-Kui, W. Dynamical behavior of ultrashort pulse laser in para-nitroaniline molecules. *Acta Phys. Sin.* **2005**, *54*, 2072−2078.
(42) Hebestreit, M. L.; Schneider, M.; Lartian, H.; Betz, V.; Heinrich, M.; Lindic, M.; Choi, M. Y.; Schmitt, M. Structures, dipole moments and excited state lifetime of isolated 4-cyanoindole in its ground and lowest electronically excited singlet states. *Phys. Chem. Chem. Phys.* **2019**, *21*, 14766−14774.
(43) Umeyama, T.; Igarashi, K.; Sasada, D.; Tamai, Y.; Ishida, K.; Koganezawa, T.; Ohtani, S.; Tanaka, K.; Ohkita, H.; Imahori, H. Efficient light-harvesting, energy migration, and charge transfer by nanographene-based nonfullerene small-molecule acceptors exhibiting unusually long excited-state lifetime in the film state. *Chem. Sci.* **2020**, *11*, 3250−3257.
(44) Park, W.; Lee, S.; Huix-Rotllant, M.; Filatov, M.; Choi, C. H. Impact of the dynamic electron correlation on the unusually long excited-state lifetime of thymine. *J. Phys. Chem. Lett.* **2021**, *12*, 4339−4346.
(45) Beckwith, J. S.; Aster, A.; Vauthey, E. The excited-state dynamics of the radical anions of cyanoanthracenes. *Phys. Chem. Chem. Phys.* **2021**, *24*, 568−577.
(46) Gruber, E.; Teiwes, R.; Kjær, C.; Nielsen, S. B.; Andersen, L. H. Tuning fast excited-state decay by ligand attachment in isolated chlorophyll a. *Phys. Chem. Chem. Phys.* **2021**, *24*, 149−155.
(47) Zheng, G. C.; Cai, Z. B.; Pan, Y. L.; Bai, L.; Zhou, Y. T.; Li, S. L.; Tian, Y. P. Synthesis and two-photon absorption properties of novel 2-substituted-4, 5-diphenyl-1H-imidazoles. *Tetrahedron* **2016**, *72*, 2988−2996.
(48) Xu, L.; Long, X.; He, J.; Liu, L.; Kang, F.; Deng, Z.; Wu, J.; Jiang, X. F.; Wang, J.; Zhang, Q. Aggregation effects on the one-and two-photon excited fluorescence performance of regioisomeric anthraquinone-substituted perylenediimide. *J. Mater. Chem. C* **2022**, *10*, 7039−7048.

https://doi.org/10.1021/acsomega.3c01922
ACS Omega 2023, 8, 19950−19962

(49) Long, X.; Wu, J.; Yang, S.; Deng, Z.; Zheng, Y.; Zhang, W.; Jiang, X.; Lu, F.; Li, M. D.; Xu, L. Discovery of and insights into one-photon and two-photon excited ACQ-to-AIE conversion via positional isomerization. *J. Mater. Chem. C* **2021**, *9*, 11679−11689.
(50) Liang, X.; Zhang, Q. Recent progress on intramolecular charge-transfer compounds as photoelectric active materials. *Sci. China Mater.* **2017**, *60*, 1093−1101.
(51) Xu, L.; Zhang, J.; Yin, L.; Long, X.; Zhang, W.; Zhang, Q. Recent progress in efficient organic two-photon dyes for fluorescence imaging and photodynamic therapy. *J. Mater. Chem. C* **2020**, *8*, 6342−6349.
(52) Xu, L.; Lin, W.; Huang, B.; Zhang, J.; Long, X.; Zhang, W.; Zhang, Q. The design strategies and applications for organic multi-branched two-photon absorption chromophores with novel cores and branches: a recent review. *J. Mater. Chem. C* **2021**, *9*, 1520−1536.

https://doi.org/10.1021/acsomega.3c01922
ACS Omega 2023, 8, 19950−19962